International Journal of Energy Research

INTERNATIONAL JOURNAL OF ENERGY RESEARCH
Int. J. Energy Res. 2015; **39**:573–584
Published online 19 December 2014 in Wiley Online Library (wileyonlinelibrary.com). DOI: 10.1002/er.3274

Modeling of steady-state and transient thermal performance of a Li-ion cell with an axial fluidic channel for cooling

K. Shah and A. Jain*,†

Mechanical and Aerospace Engineering Department, University of Texas at Arlington, Arlington, TX, USA

SUMMARY

Thermal management of Li-ion cells is an important technological problem for energy conversion and storage. Effective dissipation of heat generated during the operation of a Li-ion cell is critical to ensure safety and performance. In this paper, thermal performance of a cylindrical Li-ion cell with an axial channel for coolant flow is analyzed. Analytical expressions are derived for steady-state and transient temperature fields in the cell. The analytical models are in excellent agreement with finite-element simulation results. The dependence of the temperature field on various geometrical and thermal characteristics of the cell is analyzed. It is shown that coolant flow through even a very small diameter axial channel results in significant thermal benefit. The trade-off between thermal benefit and reduction in cell volume, and hence capacity due to the axial channel, is analyzed. The effect of axial cooling on geometrical design of the cell, and transient thermal performance during a discharge process, is also analyzed. Results presented in this paper are expected to aid in the development of effective cooling techniques for Li-ion cells based on axial cooling. Copyright © 2014 John Wiley & Sons, Ltd.

KEY WORDS

lithium-ion cells; battery cooling; battery safety; thermal modeling

Correspondence

*Ankur Jain, Mechanical and Aerospace Engineering Department, University of Texas at Arlington, 500 W First St, Rm 211, Arlington, TX 76019, USA.

†E-mail: jaina@uta.edu

Received 20 July 2014; Revised 21 October 2014; Accepted 24 October 2014

1. INTRODUCTION

Li-ion cells have been investigated for energy conversion and storage in a wide variety of engineering applications including consumer electronics, vehicles, defense systems, etc. [1–3]. Li-ion cells offer superior energy and power density compared to other electrochemical energy storage mechanisms [1]. Within Li-ion cells, a cylindrical cell has been shown to have higher energy density than other form factors, and thus, optimization of the operation of a cylindrical cell is of much importance.

Thermal management of Li-ion cells is a significant technological challenge that must be effectively addressed for improving the performance of Li-ion cells and adoption in applications requiring aggressive rates of discharge [4–6]. Heat is generated within a Li-ion cell due to electrochemical reactions, Ohmic losses and enthalpies of various reactions and phase change processes, for which a number of theoretical models have been proposed [7–11]. The rate of heat generation is known to be a strong function of the rate at which the cell is discharged [5]. Effective removal of heat may benefit both safety and performance. Li-ion cells are remarkably temperature sensitive, and beyond a certain temperature, a thermal runaway situation may arise, which eventually leads to catastrophic failure [12,13]. To prevent such incidents, and also to improve cell performance, it is important to optimize thermal management mechanisms. Recent measurements of the thermal conductivity of cylindrical Li-ion cells have shown significant anisotropy in thermal conductivity between the radial and axial directions [4]. Steady-state and transient models for the thermal conduction within a cylindrical Li-ion cell have been developed and validated with experimental data [10,14–20]. These models highlight the importance of radial thermal conductance within the cell in determining the temperature field of the cell. One particular challenge in the cooling of cylindrical Li-ion cells is that while the radial outer surface is most commonly available for heat dissipation, thermal conductance within the cell in the radial direction is particularly poor. Cooling at the outer surfaces is likely to be ineffective for the core regions of the cell farthest away from the outer surface. Due to the relatively large axial thermal conductivity, axial conduction within the cell may provide an effective heat dissipation pathway. However, the two outer surfaces at the axial ends of the cylinder are normally used for connecting to the

Copyright © 2014 John Wiley & Sons, Ltd.

anode and cathode, and hence are not available for heat dissipation. A few papers have investigated the use of phase change materials embedded within the Li-ion cell for absorbing heat generated during operation [21]. While a phase change material may address short transient power spikes, this approach does not address the problem of steady-state thermal management of Li-ion cells. This approach may also be difficult to integrate with the manufacturing of Li-ion cells, and may interfere with the performance of the cell. Finally, inclusion of any non-electrochemical material inside the cell will reduce energy storage capacity.

A number of papers have addressed analytical modeling and prediction of steady-state and transient temperature distribution in Li-ion cells [10,14–20]. Internal temperature measurement has also been carried out using embedded thermocouples [20,22]. These papers assume a solid cell, of either cylindrical or prismatic shape, which is being cooled at the outer surfaces. It is clearly essential to explore other paradigms of heat removal from Li-ion cells. One possible approach is to provide a through-hole along the axis of the cell and flow a liquid or gas coolant through this channel. This opens up a new mechanism for heat removal which effectively reaches the core of the cell more effectively than cooling at the outer surface. Doing so, however, results in reduced cell capacity due to reduced cell volume. In view of this trade-off, it is important to carry out a comprehensive thermal analysis to fully understand the thermal benefits of coolant flow in an annular Li-ion cell, and compare these benefits with costs associated with reduced cell capacity. Such an exercise may help determine the feasibility of this thermal management approach, and develop practical guidelines for multi-physics optimization design and operation of Li-ion cells.

This paper presents analytical models for determining the steady-state and transient temperature distributions in a heat-generating annular Li-ion cell containing an axial through-hole with coolant flow. The effect of the coolant is modeled using a convective heat transfer coefficient at the inner wall. The governing energy conservation equations are solved to derive an expression for steady-state and transient temperature distributions. Results are in excellent agreement with finite-element simulations. The effect of various thermal parameters, including convective boundary conditions and precooling of the coolant, on temperature distribution is examined. It is shown that precooling provides limited benefit in thermal performance of the cell. It is shown that the provision of axial cooling reduces the cell temperature, making it possible to let the cell dissipate more heat. This provides additional thermal head that may be used to operate the cell at a higher C-rate. This can be viewed as a trade-off between the energy and power capacities of the cell. By quantifying this trade-off, this paper contributes towards a comprehensive multi-physics understanding of Li-ion cell.

The next section presents the governing energy conservation equations and a derivation of temperature distribution. Comparison with a finite-element simulation is discussed next. The effect of various thermal parameters is examined, followed by analysis of the cell size, and the energy vs. power trade-off inherent in annular Li-ion cells. Applications of these models in cell sizing and the design of transient discharge processes are analyzed.

2. ANALYTICAL MODEL

Consider an annular Li-ion cell with height H, and outer and inner radii R_o and R_i, respectively, shown schematically in Figure 1. The cell is assumed to dissipate a constant volumetric heat generation Q, which is dependent on the C-rate of the cell. The radial and axial thermal conductivities of the cell are assumed to be k_r and k_z, respectively. Assumption of anisotropic thermal conductivity is necessary based on recent measurements that show significant difference in radial and axial thermal conductivities [4]. For a general case, convective heat transfer coefficients h_{ro} and h_z are assumed at the outer surfaces in the radial ($r = R$) and axial directions ($z = 0$, $z = H$), respectively. Setting any of these to zero makes these boundary conditions adiabatic. A constant temperature boundary condition, which is easier to model, but less realistic than convective heat transfer boundary conditions can also be analyzed using methods similar to one discussed here. Coolant flow through the axial channel is modeled using a convective heat transfer coefficient h_{ri}

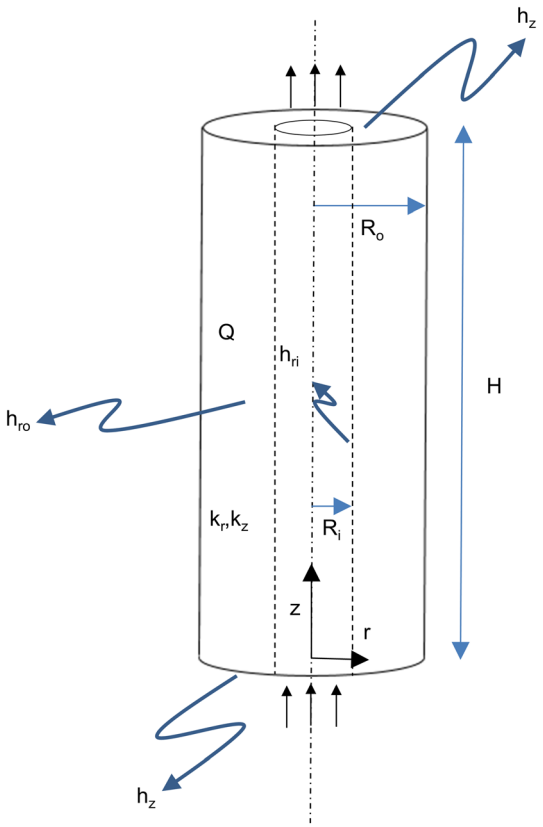

Figure 1. Schematic of geometry of the annular cell.

Int. J. Energy Res. 2015; **39**:573–584 © 2014 John Wiley & Sons, Ltd.
DOI: 10.1002/er

along the inner wall. Note that the convective heat transfer coefficients listed above are all assumed to be surface-averaged values over the respective surfaces. This significantly simplifies the analysis. Expressions for the steady-state and transient temperature distributions in the cell are derived in the following sub-sections.

2.1. Steady-state temperature distribution

The governing steady-state energy conservation equation for the annular cell is given by [23,24]

$$\frac{k_r}{r}\frac{\partial}{\partial r}\left(r\frac{\partial T}{\partial r}\right)+k_z\frac{\partial^2 T}{\partial z^2}+Q=0 \tag{1}$$

where *T(r,z)* is the temperature rise above ambient.

The governing equation is subject to the following boundary conditions [25]:

$$\frac{\partial T}{\partial z}=\frac{h_z}{k_z}T \qquad \text{at z } = 0 \tag{2}$$

$$\frac{\partial T}{\partial z}=-\frac{h_z}{k_z}T \qquad \text{at z } = H \tag{3}$$

$$\frac{\partial T}{\partial r}=\frac{h_{ri}}{k_r}(T-T_{cool}) \qquad \text{at r } = R_i \tag{4}$$

$$\frac{\partial T}{\partial r}=-\frac{h_{ro}}{k_r}T \qquad \text{at r } = R_o \tag{5}$$

Where T_{cool} is the temperature of the coolant with respect to ambient temperature. For a coolant entering at the same temperature as ambient, $T_{cool}=0$. The temperature field may be determined by first splitting *T(r,z)* into two components—one that absorbs the heat generation term, and another that accounts for other non-homogeneities. The first term is obtained in a straightforward fashion by solving its governing ordinary differential equation. The governing set of equations for the second term contains multiple non-homogeneities that can be addressed by splitting the problem into multiple sub-problems. The temperature distribution obtained using this approach is

$$T(r,z)=s(z)+w(r,z) \tag{6}$$

The two components of the temperature distribution are given by

$$s(z)=\frac{QH^2}{2k_z}\left[\frac{z}{H}\left(1-\frac{z}{H}\right)+\frac{1}{Bi_H}\right] \tag{7}$$

and

$$w(r,z)=\sum_{n=1}^{\infty}[(A_n+B_n)\cdot I_0(\lambda_n r)+(A_n\beta_1+B_n\beta_2)\cdot K_0(\lambda_n r)]\cdot[\mu_n HCos(\mu_n z)+Bi_H Sin(\mu_n z)] \tag{8}$$

The coefficients A_n and B_n in equation (8) are given by

$$A_n=\frac{-h_{ro}\int_0^H s(z)[\mu_n Cos(\mu_n z)+(h_z/k_z)Sin(\mu_n z)]dz}{\frac{1}{2}\left[(\mu_n H)^2+{Bi_H}^2+2Bi_H\right]\cdot[h_{ro}I_o(\lambda_n R_o)+k_r\lambda_n I_1(\lambda_n R_o)+\beta_1(h_{ro}K_o(\lambda_n R_o)-k_r\lambda_n K_1(\lambda_n R_o))]} \tag{9}$$

$$B_n=\frac{-h_{ri}\int_0^H (s(z)-T_{cool})[\mu_n Cos(\mu_n z)+(h_z/k_z)Sin(\mu_n z)]dz}{\frac{1}{2}\left[(\mu_n H)^2+{Bi_H}^2+2Bi_H\right]\cdot[h_{ri}I_o(\lambda_n R_i)-k_r\lambda_n I_1(\lambda_n R_i)+\beta_2(h_{ri}K_o(\lambda_n R_i)+k_r\lambda_n K_1(\lambda_n R_i))]} \tag{10}$$

where

$$\beta_1=\frac{k_r\lambda_n I_1(\lambda_n R_i)-h_{ri}I_o(\lambda_n R_i)}{k_r\lambda_n K_1(\lambda_n R_i)+h_{ri}K_o(\lambda_n R_i)} \tag{11}$$

$$\beta_2=\frac{k_r\lambda_n I_1(\lambda_n R_o)+h_{ro}I_o(\lambda_n R_o)}{k_r\lambda_n K_1(\lambda_n R_o)-h_{ro}K_o(\lambda_n R_o)} \tag{12}$$

The eigenvalues μ_n are obtained from roots of the transcendental equation

$$Tan(\mu H)=\frac{2Bi_H\cdot(\mu H)}{(\mu H)^2-{Bi_H}^2} \tag{13}$$

where Bi_H is the axial Biot number, defined as $Bi_H=\frac{h_z H}{k_z}$.

Finally,

$$\lambda_n = \sqrt{\gamma}\cdot\mu_n \tag{14}$$

where γ is the degree of anisotropy given by

$$\gamma = \frac{k_z}{k_r} \tag{15}$$

Equations (6)–(15) represent the solution for the steady-state temperature distribution in the cell.

2.2. Transient temperature distribution

The modeling of transient thermal characteristics of the annular cell is important for understanding time-dependent phenomena such as pulsed power operation, periodic or one-time spike in heat generation rate, etc. In order to account for such phenomena, the heat generation term must be considered to be time dependent. The modeling of transient temperature distribution presents additional challenges compared to steady-state modeling. The transient governing energy equation is given by

$$\frac{k_r}{r}\frac{\partial}{\partial r}\left(r\frac{\partial T}{\partial r}\right) + k_z\frac{\partial^2 T}{\partial z^2} + Q(t) = \rho C_p\frac{\partial T}{\partial t} \tag{16}$$

Where *T(r,z,t)* is the temperature rise above ambient.

The boundary conditions associated with equation (16) are the same as for the steady-state problem, equations (2)–(5) discussed in the previous section. In addition, it is assumed that the cell is at ambient temperature at t = 0, i.e. T = 0 at t = 0.

The primary difficulty in solving the transient problem arises from the heat generation term, which is a general time-dependent function. The first step towards deriving a solution for this general case is to carry out a Laplace transform of the governing energy equation and associated boundary conditions. This results in a set of partial differential equations in the Laplace space, given by

$$\frac{k_r}{r}\frac{\partial}{\partial r}\left(r\frac{\partial \overline{T}}{\partial r}\right) + k_z\frac{\partial^2 \overline{T}}{\partial z^2} + \overline{Q}(s) = \frac{\rho C_p}{s}\overline{T} \tag{17}$$

subject to

$$\frac{\partial \overline{T}}{\partial z} = \frac{h_z}{k_z}\overline{T} \qquad \text{at z} = 0 \tag{18}$$

$$\frac{\partial \overline{T}}{\partial z} = -\frac{h_z}{k_z}\overline{T} \qquad \text{at z} = H \tag{19}$$

$$\frac{\partial \overline{T}}{\partial r} = \frac{h_{ri}}{k_r}\overline{T} \qquad \text{at r} = R_i \tag{20}$$

$$\frac{\partial \overline{T}}{\partial r} = -\frac{h_{ro}}{k_r}\overline{T} \qquad \text{at r} = R_o \tag{21}$$

$\overline{T}(r,z)$and $\overline{Q}(s)$are Laplace transforms of *T(r,z,t)* and *Q(t)*, respectively. Given a certain heat generation function *Q(t)*, the function $\overline{Q}(s)$can be easily computed.

Equation (17) can be solved by splitting $\overline{T}(r,z)$ in two components. The $\overline{Q}(s)$function is absorbed in the first component, which is assumed to have axial variation only. The second part of the solution is solved using the separation of variables technique. The final solution is found to be

$$\overline{T}(r,z) = \overline{p}(z) + \overline{w}(r,z) \tag{22}$$

The first part of the solution $\overline{p}(z)$is given by

$$\overline{p}(z) = \overline{C}Sinh\left(\sqrt{\frac{\rho C_p s}{k_z}}z\right) + \overline{D}Cosh\left(\sqrt{\frac{\rho C_p s}{k_z}}z\right) \tag{23}$$

The coefficients $\overline{C}$ and $\overline{D}$ in equation (23) are determined by using boundary conditions in the z-direction, which results in

$$\overline{C} = \frac{\frac{\overline{Q}(s)}{\rho C_p s}\left(\sqrt{\rho C_p s k_z}Sinh\left(\sqrt{\frac{\rho C_p s}{k_z}}H\right) + h_z\left(Cosh\left(\sqrt{\frac{\rho C_p s}{k_z}}H\right) - 1\right)\right)}{\sqrt{\rho C_p s k_z}Cosh\left(\sqrt{\frac{\rho C_p s}{k_z}}H\right) + h_z Sinh\left(\sqrt{\frac{\rho C_p s}{k_z}}H\right) + \frac{\rho C_p s k_z}{h_z}Sinh\left(\sqrt{\frac{\rho C_p s}{k_z}}H\right) + \sqrt{\rho C_p s k_z}Cosh\left(\sqrt{\frac{\rho C_p s}{k_z}}H\right)} \tag{24}$$

$$\overline{D} = \frac{\overline{C}\sqrt{\rho C_p s k_z}}{h_z} - \frac{\overline{Q}(s)}{\rho C_p s} \tag{25}$$

The second part of the solution $\overline{w}(r,z)$ is found to be

$$\overline{w}(r,z) = \sum_{n=1}^{\infty}\left[\left(\overline{A}_n + \overline{B}_n\right)\cdot I_0(\lambda_n r) + \left(\overline{A}_n\overline{\beta}_1 + \overline{B}_n\overline{\beta}_2\right)\cdot K_0(\lambda_n r)\right]\cdot\left[\mu_n HCos(\mu_n z) + Bi_H Sin(\mu_n z)\right] \tag{26}$$

where,

DOI: 10.1002/er

$$\overline{A}_n = \frac{-h_{ro}\int_0^H \overline{p}(z)\cdot[\mu_n Cos(\mu_n z) + (h_z/k_z)Sin(\mu_n z)]dz}{\frac{1}{2}\left[(\mu_n H)^2 + Bi_H{}^2 + 2Bi_H\right]\cdot\left[h_{ro}I_o(\lambda_n R_o) + k_r\lambda_n I_1(\lambda_n R_o) + \overline{\beta}_1(h_{ro}K_o(\lambda_n R_o) - k_r\lambda_n K_1(\lambda_n R_o))\right]} \quad (27)$$

$$\overline{B}_n = \frac{-h_{ri}\int_0^H \overline{p}(z)\cdot[\mu_n Cos(\mu_n z) + (h_z/k_z)Sin(\mu_n z)]dz}{\frac{1}{2}\left[(\mu_n H)^2 + Bi_H{}^2 + 2Bi_H\right]\cdot\left[h_{ri}I_o(\lambda_n R_i) - k_r\lambda_n I_1(\lambda_n R_i) + \overline{\beta}_2(h_{ri}K_o(\lambda_n R_i) + k_r\lambda_n K_1(\lambda_n R_i))\right]} \quad (28)$$

where,

$$\overline{\beta}_1 = \frac{k_r\lambda_n I_1(\lambda_n R_i) - h_{ri}I_o(\lambda_n R_i)}{k_r\lambda_n K_1(\lambda_n R_i) + h_{ri}K_o(\lambda_n R_i)} \quad (29)$$

$$\overline{\beta}_2 = \frac{k_r\lambda_n I_1(\lambda_n R_o) + h_{ro}I_o(\lambda_n R_o)}{k_r\lambda_n K_1(\lambda_n R_o) - h_{ro}K_o(\lambda_n R_o)} \quad (30)$$

The eigenvalues μ_n are the same as eigenvalues for the steady-state problem, given by equation (13). Finally,

$$\lambda_n = \sqrt{\gamma\left(\frac{\rho C_p s}{k_z} + \mu_n{}^2\right)} \quad (31)$$

Equations (22)–(31) represent the solution for $\overline{T}(r,z)$, from where, the temperature distribution *T(r,z,t)* can be obtained from inverse Laplace transform. In case the Laplace transform is too difficult to invert explicitly, a numerical inversion technique is adopted using de Hoog's quotient difference method algorithm [26] for inverse Laplace transformation, as implemented by Hollenbeck [27].

2.3. Extension to space-dependent heat generation

The analytical derivations presented in sections 2.1 and 2.2 assumed uniform heat generation rate in the entire volume of the cell. While this is usually assumed to be the case, in general, the heat generation rate may vary with space, for example, if a short circuit causes high heat generation in a specific part of the cell. In such a case, an approach similar to one recently described for solid cells may be adopted. Briefly, if Q is a function of z, the steady-state temperature solution can be derived by accounting for Q (z) in the first part of the solution s(z) as shown in equation (6). While for uniform heat generation rate, s(z) is easily derived, for non-uniform heat generation rate, Q(z) is first written as a polynomial expansion in z. Any well-behaved function Q(z) can be written as a polynomial expansion as follows

$$Q(z) = \sum_{n=0}^{\infty} c_n\left(\frac{z}{H}\right)^n \quad (32)$$

Following this, s(z) can be determined by twice integrating the governing ordinary differential equation that contains the polynomial expansion for Q(z). The second part of the solution, w(r,z), given by equation (8) remains unchanged.

3. COMPARISON WITH FINITE-ELEMENT SIMULATION

In order to validate the model presented in Section 2, the temperature distribution computed from the model is compared with finite-element simulations. Figure 2 plots the steady-state temperature computed using equations (6)–(15) as a function of the radial coordinate at mid-height. The cell considered here has the same outer dimensions as a 26650 cell, but has an axial hole of radius 2.6 mm. The convective heat transfer coefficients are assumed to be $h_{ri} = 1000\ \mathrm{W/m^2K}$, $h_{ro} = 100\ \mathrm{W/m^2K}$ and $h_z = 100\ \mathrm{W/m^2K}$. Based on recent measurements [4], the thermal conductivities of the cell are assumed to be $k_r = 0.2\ \mathrm{W/mK}$ and $k_z = 30\ \mathrm{W/mK}$, respectively. The cell is assumed to dissipate 6-W power. The temperature distribution predicted by a finite-element simulation software is also plotted, and there is excellent agreement between the two. The negligible error between the two occurs due to truncation errors in the respective computations. Figure 3 plots the temperature computed using equations (22)–(31) at the center of the cell material at mid-height as a function of time. The value of R_i is taken to be 2.6 mm, and all other parameters are the same as Figure 2. Similar to Figure 2, there is good agreement between the transient model and finite-element simulation results.

Compared to the finite-element simulation, the analytical model presented in Section 2 is capable of computing temperature much faster, only a few seconds for the entire temperature distribution in the cell, compared to several minutes for a typical finite-element simulation tool, without even accounting for time needed to set up and mesh the problem geometry. Moreover, the analytical model

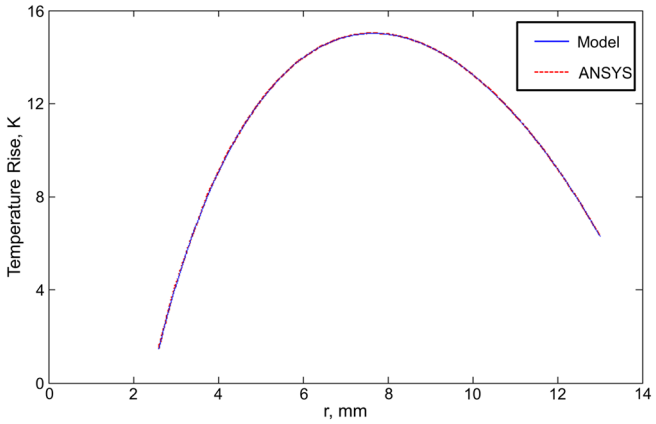

Figure 2. Comparison of temperature distribution as a function of r predicted by the steady-state model with finite-element simulation results.

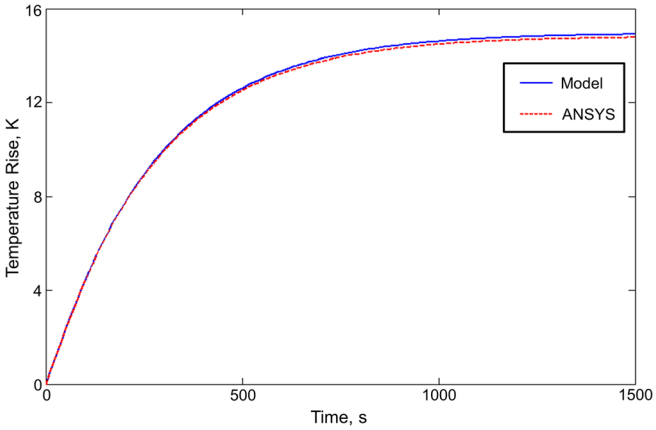

Figure 3. Comparison of peak cell temperature as a function of time predicted by the transient model with finite-element simulation results.

provides a fundamental understanding of thermal characteristics of the annular cell, and facilitates rapid parametric studies of the effect of different variables on the temperature distribution.

4. RESULTS AND DISCUSSION

The analytical model presented in Section 2 is used for developing an understanding of the effect of various parameters on the temperature distribution in the annular cell, and to examine various trade-offs in the thermal design of an annular cell.

Figures 4(a) and 4(b) plot the radial temperature distribution at mid-height as function of the inner radius R_i, and the inner convective heat transfer coefficient h_{ri}, respectively, for fixed outer geometry of the cell. In Figure 4 (a), h_{ri} is held constant at 1000 W/m^{2}K, and in Figure 4(b), R_i is held constant at 2.6 mm. Figure 4(a) shows that as the inner radius increases, there is a substantial reduction in peak temperature rise. The peak temperature rise for an equivalent solid cell without an axial channel is 30.0 °C, also shown in Figure 4(a). In addition to temperature reduction, there is also a shift in the location where the peak temperature rise occurs. The greater the inner radius, the farther out is the location of peak temperature rise. Figure 4(b) shows, as expected, that for a given cell geometry, increasing the convective heat transfer coefficient h_{ri} reduces the peak temperature rise. A larger value of h_{ri} could be obtained, for example, by increasing the flow rate or thermal conductivity of the coolant.

Another possible strategy to reduce temperature rise through axial cooling is to precool the coolant prior to entering the annular cylinder. Figure 5 plots radial temperature distributions at mid-height when the coolant is precooled by different temperatures. Figure 5 shows that precooling may not be a particularly effective strategy for cooling of Li-ion cells. For example, precooling the coolant by 10 °C results in a peak temperature reduction of less than 5 °C. Precooling offers the advantage that it partially shifts the cooling load from the cell to the coolant, which in most cases is likely to be easier to implement, for

Int. J. Energy Res. 2015; **39**:573–584 © 2014 John Wiley & Sons, Ltd.
DOI: 10.1002/er

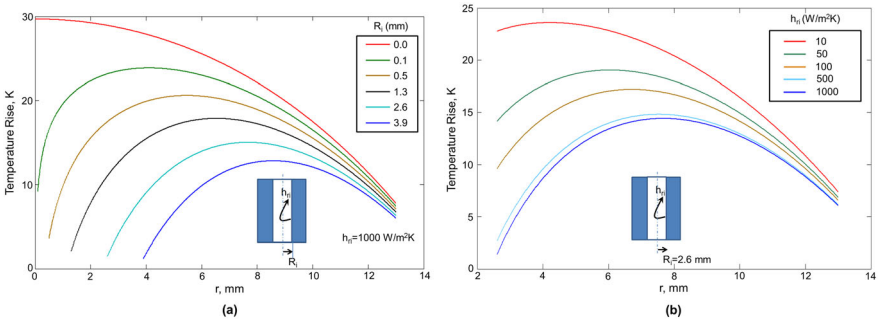

Figure 4. (a) Steady-state temperature as a function of r for different values of R_i at fixed h_{ri}; (b) steady-state temperature as a function of h_{ri} for different values of R_i at fixed R_i.

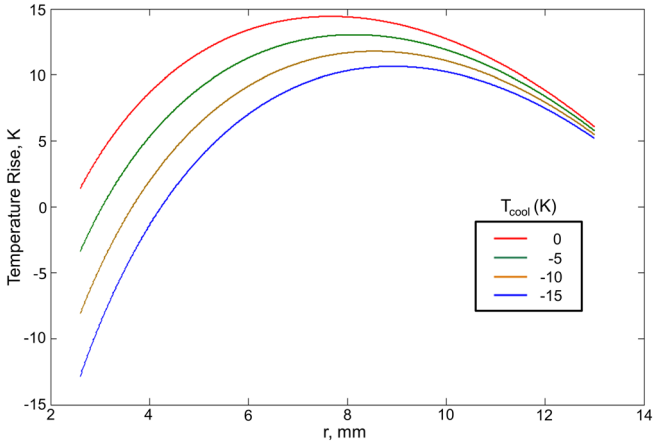

Figure 5. Temperature distribution in the annular cell as a function of extent of precooling of the coolant fluid.

example by using a remotely located chiller. It is possible in certain applications where performance is critical, and the cost of precooling is acceptable, that precooling may be an attractive option.

One fundamental thermal-electrical trade-off that active cooling of an annular Li-ion cell must address is the trade-off between reduction in cell temperature and reduction in cell capacity. By increasing the inner radius of the annular cylinder, it is possible to reduce the cell temperature due to increased coolant flow. However, this also results in reduction in capacity of the cell since the increased coolant flow region reduces the cell volume and hence the cell capacity. This trade-off is analyzed in Figure 6, which plots the peak temperature rise in the cell and total capacity as functions

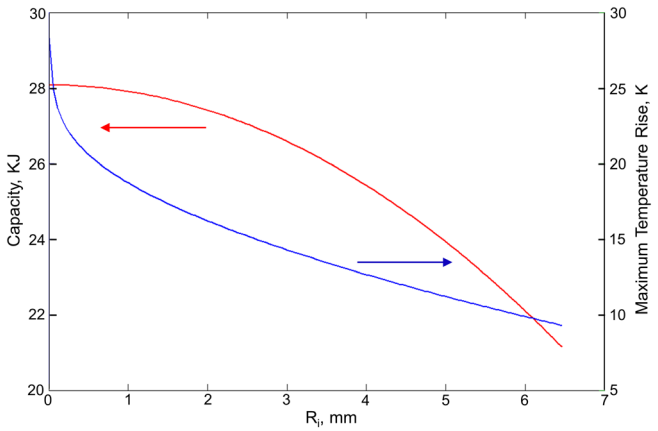

Figure 6. Cell capacity and peak temperature rise as functions of inner radius R_i.

of the inner radius of the cell. The heat generation rate in the cell is assumed to stay the same at 6 W. The baseline case considered here is that of a 26650 cell that delivers 2.6 A-h charge at 3.0 V, resulting in a total energy capacity of 28080 J. It is assumed that the capacity scales with the cell volume, since the volume directly influences that total volume of electrodes within the cell, thus affecting the capacity of the cell. It is seen that increasing the inner radius results in rapid temperature reduction. The temperature curve in Figure 6 is very steep at low R_i. This indicates that even an axial hole of very small diameter results in significant temperature reduction with negligible reduction in capacity. For example, an annular cell with $R_i = 0.1$ mm results in a temperature rise of only 24 °C compared to a 30 °C temperature rise for an equivalent 26650 cell without an axial channel. At the same time, the reduction in cell capacity due to the axial channel is negligible. At a somewhat larger value of $R_i = 1.3$ mm, the reduction in capacity is still only 1% whereas there is a 40% reduction in peak temperature compared to the equivalent cell without an axial channel. However, as R_i increases, the cell capacity also reduces, due to which the trade-off between capacity reduction and improved thermal performance must be analyzed in detail. A reduction in peak temperature rise of a cell due to active cooling presents a direct opportunity to improve the electrical performance of the cell. The thermal head provided by the reduced cell temperature enables, for example an increase in the C-rate of the cell. The C-rate of the cell can be increased in order to reach the baseline temperature rise. This opportunity enabled by active cooling, however, comes at the cost of reduced cell capacity. Thus, active cooling can be thought of as a means to balance the trade-off between capacity and power of a Li-ion cell. Figure 7 examines this by plotting the total capacity and C-rate as functions of the inner radius R_i, while keeping all other parameters constant. In particular, the C-rate is chosen in order to maintain the same peak temperature rise of 30 °C. The heat generation rate in the cell is modeled to vary as the square of the C-rate, or discharge current. That is,

$$Q = I^2 r_{\text{int},eff} \tag{33}$$

Where $r_{int,eff}$ is the effective internal resistance of the cell that determines the heat generation rate. Note that $r_{int,eff}$ absorbs a number of disparate heat generation mechanisms that occur inside the cell, including Ohmic losses, entropic heating, heats of reactions, etc. [10,11]. In Figures 6 and 7, a Li-ion cell with a capacity of 2.6 A-h is assumed for calculating the C-rate. Figure 7 shows that by increasing the radius of the axial channel in the Li-ion cell, the C-rate of the cell can be increased significantly without any increase in operating temperature. Even small R_i results in significant potential for C-rate improvement. However, even with R_i as small as 1.3 mm, the C-rate can be 7.7 compared to the baseline C-rate of 6.0 for a solid cell, with minimal reduction in cell capacity.

The improvement in C-rate due to effective cooling, as demonstrated in Figure 7 is also a function of h_{ri}, the convective heat transfer coefficient available at the inner wall of the cell where heat is convected out from the cell into the cooling fluid. Improvement in h_{ri} can be brought about by increasing coolant flowrate, increasing coolant thermal conductivity, etc. Improvement in h_{ri} is expected to result in reduced temperature, and hence increased C-rate to maintain the same baseline temperature. Figure 8 plots the maximum possible C-rate as a function of h_{ri} and shows that initially, C-rate increases rapidly with increasing h_{ri}. This effect, however, diminishes at large values of h_{ri}, and the improvement obtained in C-rate is minimal a value of h_{ri} of about 300 W/m^{2}K. This is because at large h_{ri}, convection to the coolant fluid is no longer the thermal bottleneck, and hence further improvement in h_{ri} does not any more result in significant further improvement in C-rate.

Given the critical importance of limiting temperature rise in Li-ion cells in order to prevent thermal runaway, it may be acceptable to sacrifice some capacity in return for improved thermal performance, which as shown in Figures 6 and 7 may in turn be used to increase discharge rates. Other challenges that may need to be considered in

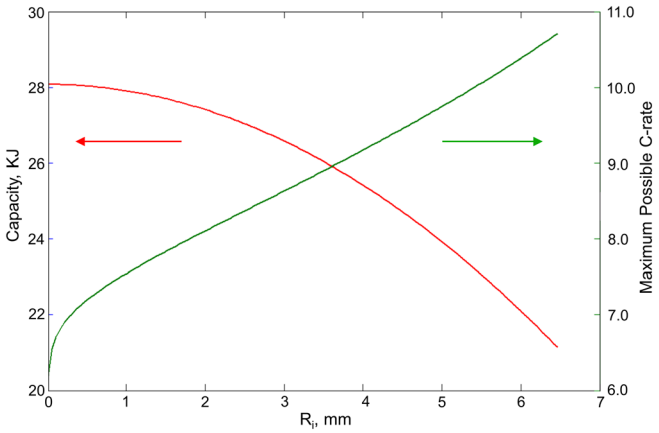

Figure 7. Maximum possible C-rate and cell capacity as function of inner radius R_i.

Int. J. Energy Res. 2015; **39**:573–584 © 2014 John Wiley & Sons, Ltd.
DOI: 10.1002/er

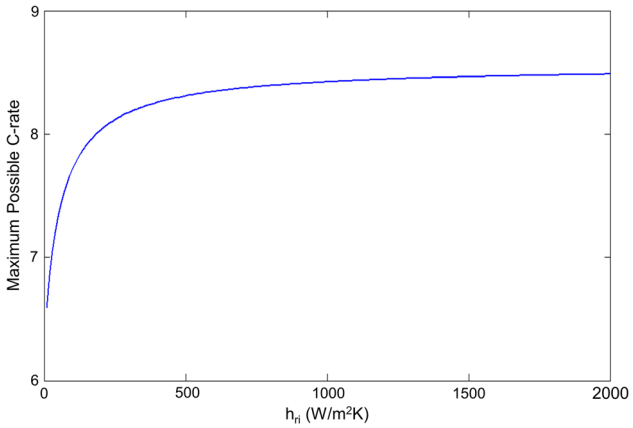

Figure 8. Maximum possible C-rate as a function of h_{ri} for fixed R_i.

the system-level analysis of this trade-off include the pumping power required to flow coolant through the axial channel, which can be large particularly for small sized channels, sealing of the channel, and its effect on the electrochemistry of the cell.

Figure 9 analyzes the effect of the overall shape of the annular Li-ion cell on maximum temperature rise in the cell, which is plotted as a function of the outer radius R_o. The overall volume of the cell is maintained constant, in this case equal to the volume of the 26650 cell. As R_o increases, the cell becomes shorter and stouter. In each case, R_i is maintained at 20% of R_o. Figure 9 shows that as R_o increases, the peak temperature of the cell increases until a worst-case value of R_o beyond which the temperature reduces. This phenomenon occurs because as R_o changes, the surface area, and hence the rate of convective heat transfer from cell to the ambient changes. The worst-case value of R_o can be thought of as one at which the available convective surface area is the minimum, resulting in worst conditions for convective heat loss from the cell. Figure 9 indicates that tall and slender cells may in general be thermally more attractive.

Figures 10 and 11 present applications of the transient model discussed in Section 2.2. The case of a discharging annular Li-ion cell is considered. Figure 10 considers a transient scenario where there is a sudden in heat generation rate in a Li-ion cell, possibly due to short circuiting. The heat generation rate is assumed to rise from 6 W to 12 W for a period of 50 s. The variation of temperature with time, computed using the model in Section 2.2, shows a sudden spike in the rate at which temperature increases. Once the heat generation rate returns to baseline value, so does the rate of increase in temperature.

In Figure 11, the cell is assumed to discharge a specific amount of energy, 3000 J in this case. Three different cases are considered with different C-rates, due to which heat dissipation of the cell and duration of discharge vary. For discharge at a high C-rate, the heat generation rate is large, while the discharge duration is small. On the other hand, discharge at a low C-rate results in lower heat generation,

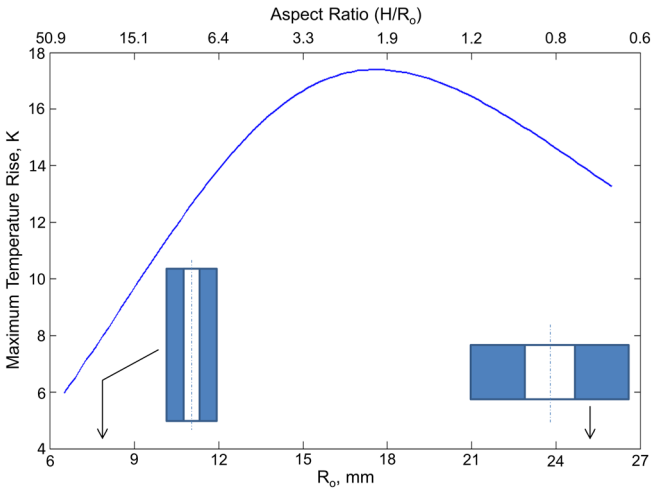

Figure 9. Effect of cell sizing on thermal performance of the annular cell.

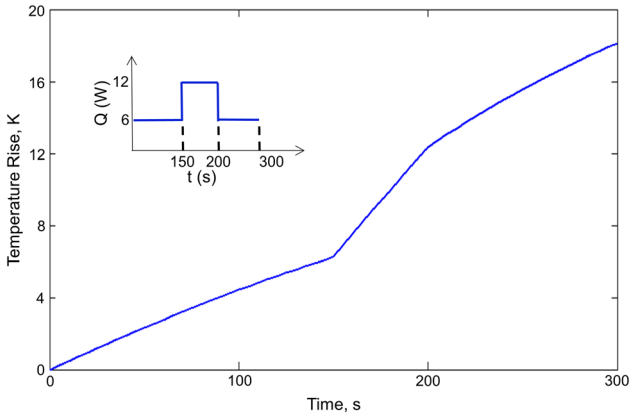

Figure 10. Computed temperature at the center of the cell material as a function of time for a short time excursion in heat generation rate.

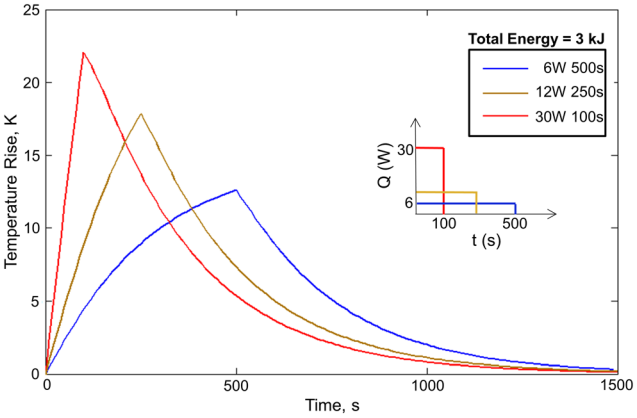

Figure 11. Peak cell temperature as a function of time for pulsed discharge processes at different rates, with fixed total discharge energy.

but longer duration for the heat generation. The peak temperature of the cell is plotted as a function of time during these discharge processes. It is found that despite the shorter discharge duration, the peak temperature rise in the high power discharge case is the highest. This indicates that from a thermal perspective, it is preferable to discharge at low rates, even if the discharge lasts for a longer duration. Note, however, that a longer duration discharge reduces overall system throughput, since each discharge process takes a long time. Figure 11 quantifies a typical thermal vs. performance trade-off that must be considered in the design of the operation of annular Li-ion cells.

The availability of analytical tools to predict steady-state and transient temperature distribution in Li-ion cells could be used by the Battery Management System (BMS) to take smart, thermal-based decisions to maximize system-level performance without overheating. For example, based on current loads, the BMS can predict when a particular cell is close to overheating, and can accordingly reduce load at the appropriate time.

Note that in addition to cooling of a cell during operation, it may also be possible to flow warm fluid through the fluid channel to warm up the cell prior to operation in low ambient temperature. This may be relevant to startup of electric/hybrid vehicles in extreme cold weather.

5. CONCLUSIONS

This paper presents analytical models for predicting steady-state and transient temperature distributions in a cylindrical Li-ion cell with a fluidic channel along the axis for cooling. Axial cooling offers several advantages compared to other approaches for thermal management of a Li-ion cell. The models presented here quantify the cooling benefit to be expected from this approach as a function of various parameters. Results indicate that axial cooling can be used to modulate the capacity vs. power trade-off in the cell. In particular, a large channel results in more cooling, making it possible to operate the cell at a larger C-rate, at the expense of slightly reduced cell capacity

Int. J. Energy Res. 2015; **39**:573–584 © 2014 John Wiley & Sons, Ltd.
DOI: 10.1002/er

due to reduced cell volume. While results presented here may facilitate thermally driven safe and high performance operation, several system-level integration challenges will also need to be addressed in the future.

NOMENCLATURE

Bi_H	= Axial Biot number
H	= Height of annular Li-ion cell (mm)
h_{ri}	= Radial (inner) convective heat transfer coefficient ($W/m^2 \cdot K$)
h_{ro}	= Radial (outer) convective heat transfer coefficient ($W/m^2 \cdot K$)
h_z	= Axial convective heat transfer coefficient ($W/m^2 \cdot K$)
I	= Discharge/charge current (A)
k_r	= Radial thermal conductivity (W/m·K)
k_z	= Axial thermal conductivity (W/m·K)
Q	= Volumetric geat generation (W/m^3)
R_i	= Inner radii of annular Li-ion cell (mm)
r_{inteff}	= Effective internal resistance of the cell (Ω)
R_o	= Outer radii of annular Li-ion cell (mm)
T	= Temperature rise above ambient (K)
T_{cool}	= Temperature of coolant with respect to ambient temperature (K)
μ	= Eigenvalues (1/m)
γ	= Degree of anisotropy

REFERENCES

1. Armand M, Tarascon J-M. Building better batteries. *Nature* 2008; **451**:652–657.
2. Scrosati B, Garche J. Lithium batteries: Status, prospects and future. *Journal of Power Sources* 2010; **9**: 2419–2430.
3. Khaligh A, Li Z. Battery, ultracapacitor, fuel cell, and hybrid energy storage systems for electric, hybrid electric, fuel cell, and plug-in hybrid electric vehicles: State of the art. *IEEE Trans Vehicular Technology* 2010; **59**:2806–2814.
4. Drake SJ, Wetz DA, Ostanek JK, Miller SP, Heinzel JM, Jain A. Measurement of anisotropic thermophysical properties of cylindrical Li-ion cells. *Journal of Power Sources* 2014; **252**:298–304.
5. Bandhauer TM, Garimella S, Fuller T. A critical review of thermal issues in Lithium-ion batteries. *Journal of the Electrochemical Society* 2011; **158**:R1–R25.
6. Karimi G, Li X. Thermal management of lithium-ion batteries for electric vehicles. *International Journal of Energy Research* 2013; **37**:13–24.
7. Srinivasan V, Wang CY. Analysis of electrochemical and thermal behavior of Li-ion cells. *Journal of the Electrochemical Society* 2003; **150**:A98–A106.
8. Abdul-Quadir Y, Laurila T, Karppinen J, Jalkanen K, Vuorilehto K, Skogström L, Paulasto-Kröckel M. Heat generation in high power prismatic Li-ion battery cell with LiMnNiCoO2 cathode material. *International Journal of Energy Research* 2014; **38**:1424–1437.
9. Thomas KE, Newman J. Heats of mixing and of entropy in porous insertion electrodes. *Journal of Power Sources* 2003; **119**:844–849.
10. Chen Y, Evans JW. Heat Transfer Phenomena in Lithium/Polymer-Electrolyte Batteries for Electric Vehicle Application. *Journal of the Electrochemical Society* 1993; **140**:1833–1838.
11. Bernardi D, Pawlikowski E, Newman J. A General Energy Balance for Battery Systems. *Journal of the Electrochemical Society* 1985; **132**:5.
12. Lisbona D, Snee T. A review of hazards associated with primary lithium and lithium-ion batteries. *Process Safety and Environmental Protection* 2011; **89**: 434–442.
13. Feng ZC, Zhang Y. Thermal runaway due to symmetry breaking in parallel-connected battery cells. *International Journal of Energy Research* 2014; **38**:813–821.
14. Shah K, Drake SJ, Wetz DA, Ostanek JK, Miller SP, Heinzel JM, Jain A. Modeling of steady-state convective cooling of cylindrical Li-ion cells. *Journal of Power Sources* 2014; **258**:374–381.
15. Shah K, Drake SJ, Wetz DA, Ostanek JK, Miller SP, Heinzel JM, Jain A. An Experimentally Validated Transient Thermal Model for Cylindrical Li-ion Cells. *Journal of Power Sources*, 2014; **271**:262–268.
16. Chen SC, Wan CC, Wang YY. Thermal analysis of Lithium-ion batteries. *Journal of Power Sources* 2005; **140**:111–124.
17. Taheri P, Bahrami M. Temperature rise in prismatic polymer lithium-ion batteries: An analytic approach. *SAE International Journal Passanger Cars* 2012; **5**:164–176.
18. Taheri P, Yazdanpour M, Bahrami M. Transient three-dimensional thermal model for batteries with thin electrodes. *Journal of Power Sources* 2013; **243**:280–289.
19. Fang W, Kwon OJ, Wang C-Y. Electrochemical–thermal modeling of automotive Li-ion batteries and experimental validation using a three-electrode cell. *International Journal of Energy Research* 2010; **34**:107–115.
20. Forgez C, Do DV, Friedrich G, Morcrette M, Delacourt C. Thermal modeling of a cylindrical LiFePO4 /graphite lithium-ion battery. *Journal of Power Sources* 2010; **195**:2961–2968.
21. Sabbah R, Kizilel R, Selman JR, Al-Hallaj S. Active (air-cooled) vs. passive (phase change material)

thermal management of high power lithium-ion packs: Limitation of temperature rise and uniformity of temperature distribution. J. *Power Sources* 2008; **182**:630–638.
22. Zhang G, Cao L, Ge S, Wang C-Y, Shaffer CE, Rahn CD. In situ measurement of radial temperature distributions in cylindrical Li-ion cells. *Journal of the Electrochemical Society* 2014; **161**:A1499–A1507.
23. Özişik N. *Heat conduction* (2nd). John Wiley & Sons: Oxford, United Kingdom, 1993.
24. Carslaw HS, Jaegar JC. *Conduction of heat in solids* (2nd). Clarendon Press: Hoboken, NJ, 1959.
25. Kays WM, Crawford ME. '*Convective Heat and Mass Transfer*,' 3rd Ed. McGraw-Hill: New York, NY, 1993.
26. de Hoog FR, Knight JH, Stokes AN. An improved method for numerical inversion of Laplace transforms. *S.I.A.M. Journal on Scientific and Statistical Computing* 1982; **3**:357–366.
27. Hollenbeck KJ. INVLAP.M: A matlab function for numerical inversion of Laplace transforms by the de Hoog algorithm, 1998, available at http://www.isva.dtu.dk/staff/karl/invlap.htm, accessed 1/01/2012.